Supporting Information

Selective Extraction of C_{70} by a Tetragonal Prismatic Porphyrin Cage

Yi Shi,[1,#] Kang Cai,[1,#] Hai Xiao,[2] Zhichang Liu,[1,3] Jiawang Zhou,[1] Dengke Shen,[1] Yunyan Qiu,[1] Qinghui Guo,[1] Charlotte Stern,[1] Michael R. Wasielewski,[1] François Diederich,[4] William A. Goddard III,[2] and J. Fraser Stoddart[1,5,6,*]

[1] *Department of Chemistry, Northwestern University, 2145 Sheridan Road, Evanston, Illinois 60208, USA*

[2] *Materials and Process Simulation Center, California Institute of Technology, Pasadena, California 91125, USA*

[3] *Institute of Natural Sciences, Westlake Institute for Advanced Study, Westlake University, No. 18 Shilongshan Road, Xihu District, Hangzhou 310064, P. R. China.*

[4] *Laboratory of Organic Chemistry, ETH Zurich, Vladimir-Prelog-Weg 3, CH-8093 Zurich, Switzerland*

[5] *Institute for Molecular Design and Synthesis, Tianjin University, Tianjin 300072, P. R. China*

[6] *School of Chemistry, University of New South Wales, Sydney, NSW 2052, Australia.*

*E-mail: stoddart@northwestern.edu

Section A. General Methods

All reagents were purchased from commercial suppliers and used without further purification. Thin layer chromatography (TLC) was performed on silica gel 60 F254 (E. Merck). Column chromatography was carried out on silica gel 60F (Merck 9385, 0.040–0.063 mm). UV-Vis Spectra were recorded at room temperature on a Shimadzu UV-3600 spectrophotometer. Fluorescence quantum yield was acquired using HORIBA Nanolog spectrofluorimeter and perylene in EtOH as reference. All samples were dissolved in CH_2Cl_2 and the excitation wavelength was 420 nm. Nuclear magnetic resonance (NMR) spectra were recorded on a Bruker Avance III 500 MHz and 600 MHz spectrometers, with working frequencies of 600 and 500 MHz (^{1}H NMR), respectively, and at 150 and 125 MHz (^{13}C NMR), respectively. Chemical shifts were reported in ppm relative to the signals corresponding to the residual non-deuterated solvents (CD_3CN: δ_H = 1.94 ppm and δ_C = 118.26 ppm; $CDCl_3$: δ_H = 7.26 ppm and δ_C = 77.16 ppm; CD_3SOCD_3: δ_H = 2.50 ppm and δ_C = 39.52 ppm; $(CD_3)_2NCOD$: δ_H = 2.75, 2.92, and 8.03 ppm and δ_C = 29.76, 34.89, and 163.15 ppm). High-resolution mass spectra were measured on an Agilent 6210 Time-of-Flight (TOF) LC-MS, using an ESI source, coupled with Agilent 1100 HPLC stack, using direct infusion (0.6 mL/min). Measurements at X-band (9.5 GHz) were performed with a Bruker Elexsys E580, equipped with a variable Q dielectric resonator (ER-4118X-MD5-W1). Single crystal X-ray diffraction data were collected using a Bruker diffractometer equipped with a Kappa goniometer, microfocus CuKα source, MX optics, and an Apex2 CCD area detector. Elaborations on the above experimental details are provided below in the appropriate sections.

Section B. Synthetic Protocols

1) Synthesis of the 5,10,15,20-tetrakis(3-(bromomethyl)phenyl)porphyrin (bzTPP)

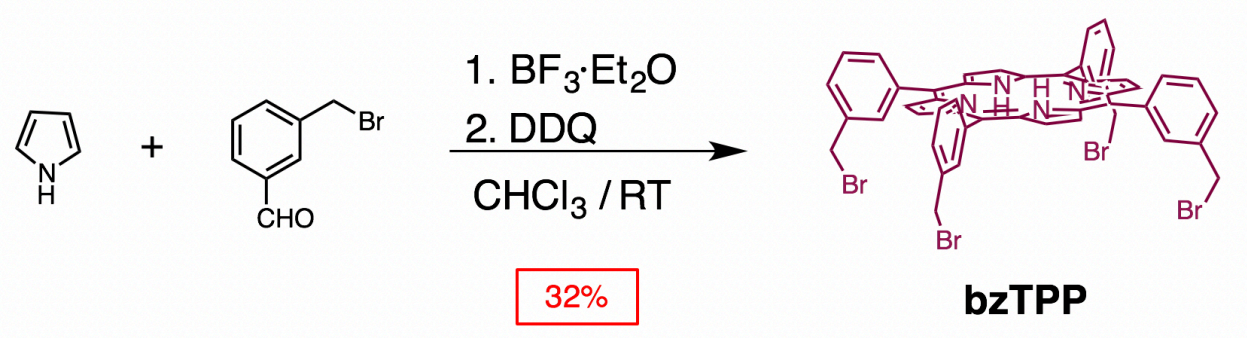

Scheme S1. Synthesis of the **bzTPP**

3-(Bromomethyl)benzaldehyde (1.9 g, 10 mmol) and pyrrole (0.7 mL, 10 mmol) were dissolved in a mixture of EtOH (5 ml) and CH_2Cl_2 (700 mL). The solution was deoxygenated under a stream of N_2 for 15 min. BF_3OEt_2 (0.37 ml, 3 mmol) was added, immediately turning the solution a golden yellow color. The reaction was protected from light and stirred for 3 h, then DDQ (1.7 g, 7.5 mmol) was added and stirring continued for a further 1 h. The reaction was neutralized with Et_3N (0.55 mL, 4 mmol) and the solution condensed under reduced pressure. The crude mixture was purified on silica eluting with CH_2Cl_2. The solvent was removed on a rotary evaporator to yield the product as a purple-black microcrystalline solid (750 mg, 30%). ^{1}H NMR (500 MHz, $CDCl_3$, ppm): δ 8.89 (s, 8H), 8.28 (s, 4H), 8.18 (d, J = 7.4 Hz, 4H), 7.83 (d, J = 7.9 Hz, 4H), 7.74 (t, J = 7.7 Hz, 4H), 4.79 (s, 8H), –2.77 (s, 2H). ^{13}C NMR (126 MHz, $CDCl_3$, ppm): δ 142.7, 136.6, 135.2, 134.7, 128.6, 127.4, 119.7, 33.7. ESI-HRMS for **bzTPP**; Calcd for $C_{48}H_{35}Br_4N_4$: m/z = 986.9554 $[M + H]^+$; found: 986.9546.

2) Synthesis of the TB•4PF$_6$

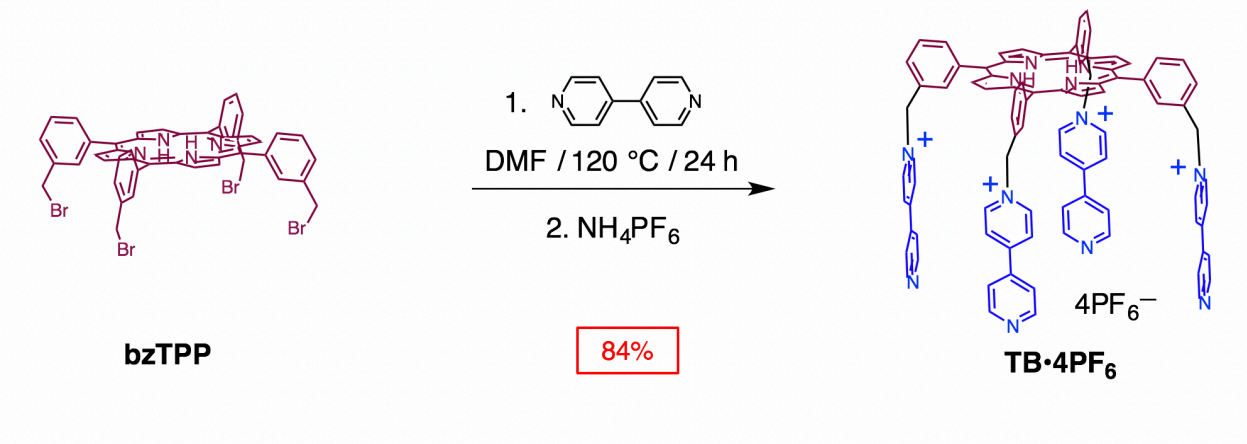

Scheme S2. Synthesis of the **TB**•4PF$_6$

4,4'-Bipyridine (20.0 equiv, 15.6g, 10 mmol) was added to a solution of **bzTPP** (491mg, 0.5 mmol) in DMF (100 mL). After heating at 120 °C for 1 d, the mixture was cooled to room temperature and concentrated on a rotary evaporator under reduced pressure. The mixture was poured into CH_2Cl_2, and the resulted precipitate was collected by filtration and washed with CH_2Cl_2. Next, the purple solid was dissolved in H_2O and the insoluble brown solid removed upon filtration. Counterion exchange was accomplished by the addition of aqueous saturated NH_4PF_6 solution, resulting in the precipitation of pure **TB**•4PF$_6$ (785 mg, 84%) that was collected by filtration as a purple solid. ^{1}H NMR (500 MHz, CD_3CN, ppm): δ 9.03 (d, J = 4.7 Hz, 8H), 8.87 – 8.83 (m, 16H), 8.38 – 8.27 (m, 16H), 7.96 – 7.90 (m, 8H), 7.78 – 7.76 (m, 8H), 6.05 (s, 8H), -2.95 (s, 2H). ^{13}C NMR (125 MHz, CD_3CN, ppm): δ 155.6, 152.1, 146.1, 143.7, 142.1, 136.5, 135.5, 132.8, 129.8, 129.1, 127.3, 122.8, 120.3, 65.1. ESI-HRMS for **TB**•4PF$_6$; Calcd for $C_{88}H_{66}F_{12}N_{12}P_2$: *m/z* = 790.7419 $[M - 2\ PF_6]^{2+}$; found: 790.7416.

3) Synthesis of the TPPCage·8PF$_6$

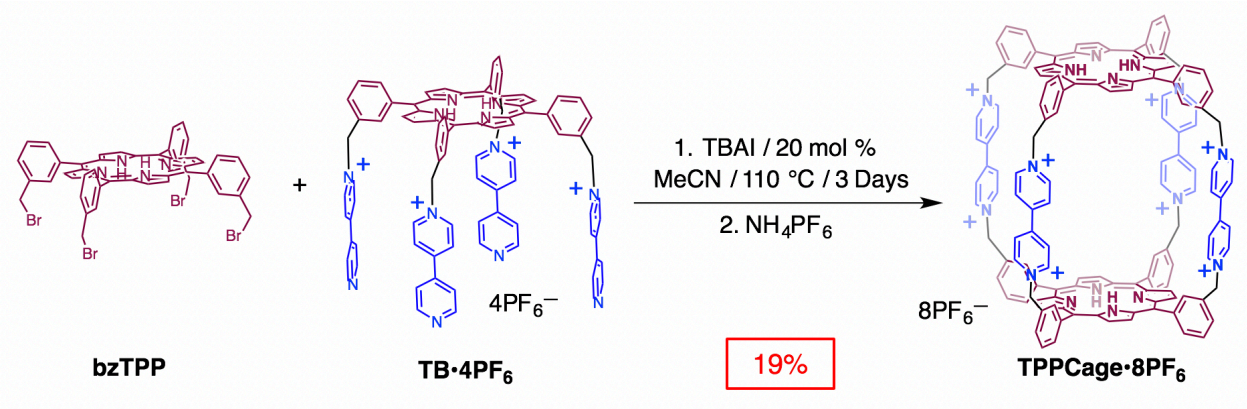

Scheme S3. Synthesis of the **TPPCage**·8PF$_6$

A solution of **TB**•4PF$_6$ (187 mg, 0.1 mmol, 1 equiv), **bzTPP** (98 mg, 0.1 mmol, 1 equiv), and tetra-*n*-butylammonium iodide (TBAI, 7 mg, 0.2 equiv) in dry MeCN (150 mL) was stirred at 110 °C for 3 d. After cooling down to room temperature, the resulting precipitate was collected by centrifugation. The green solid was dissolved in H_2O, followed by the addition of aqueous saturated NH_4PF_6 solution, resulting in the precipitation of **TPPCage**•8PF$_6$ (59 mg, 19%) which was collected by centrifugation as a green solid. ^{1}H NMR (500 MHz, $(CD_3)_2NCDO$, ppm) δ 9.63 (d, J = 6.7 Hz, 16H), 8.88 (s, 16H), 8.65 (d, J = 6.7 Hz, 16H), 8.36 (d, J = 7.5 Hz, 8H), 8.25 (d, J = 8.0 Hz, 8H), 8.22 (s, 8H), 8.05 – 8.02 (m, 8H), 6.51 (s, 16 H), -3.20 (s, 4 H). ^{13}C NMR (125 MHz, $(CD_3)_2NCDO$, ppm): δ 150.9, 147.5, 143.6, 137.6, 136.1, 133.1, 131.2, 129.3, 128.1, 120.6, 65.2. ESI-HRMS for **TPPCage**•8PF$_6$; Calcd for $C_{136}H_{100}F_{48}N_{16}P_8$: m/z = 1413.8095 $[M - 2\ PF_6]^{2+}$; found: 1413.8092.

Section C. NMR Spectroscopy

1) ^{1}H NMR Spectra of TPPCage·8PF$_6$

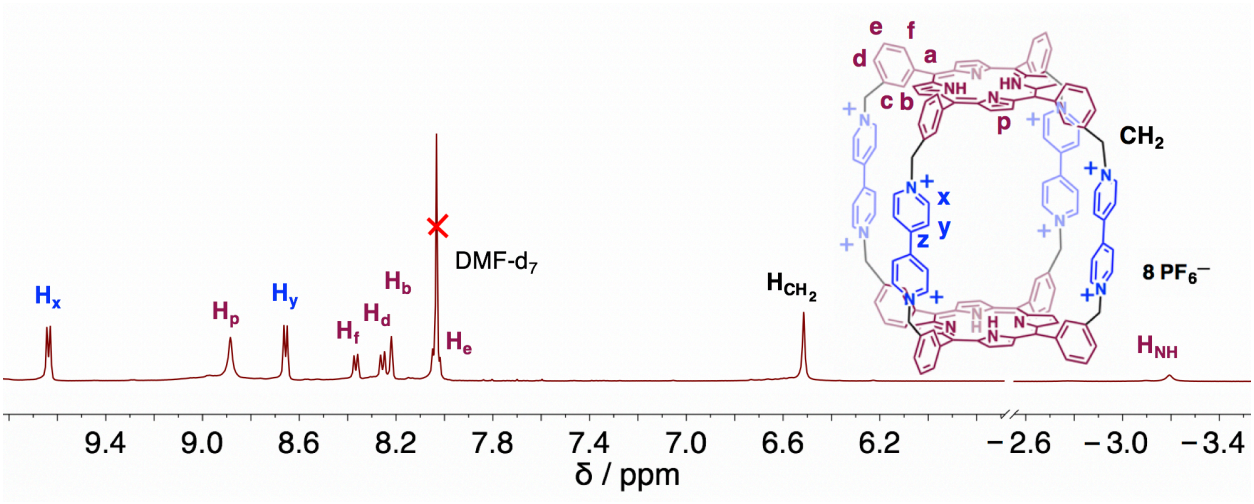

Figure S1. ^{1}H NMR Spectrum (500 MHz, DMF-d_7, 298 K) of **TPPCage**·8PF$_6$.

2) ^{13}C NMR Spectra of TPPCage·8PF$_6$

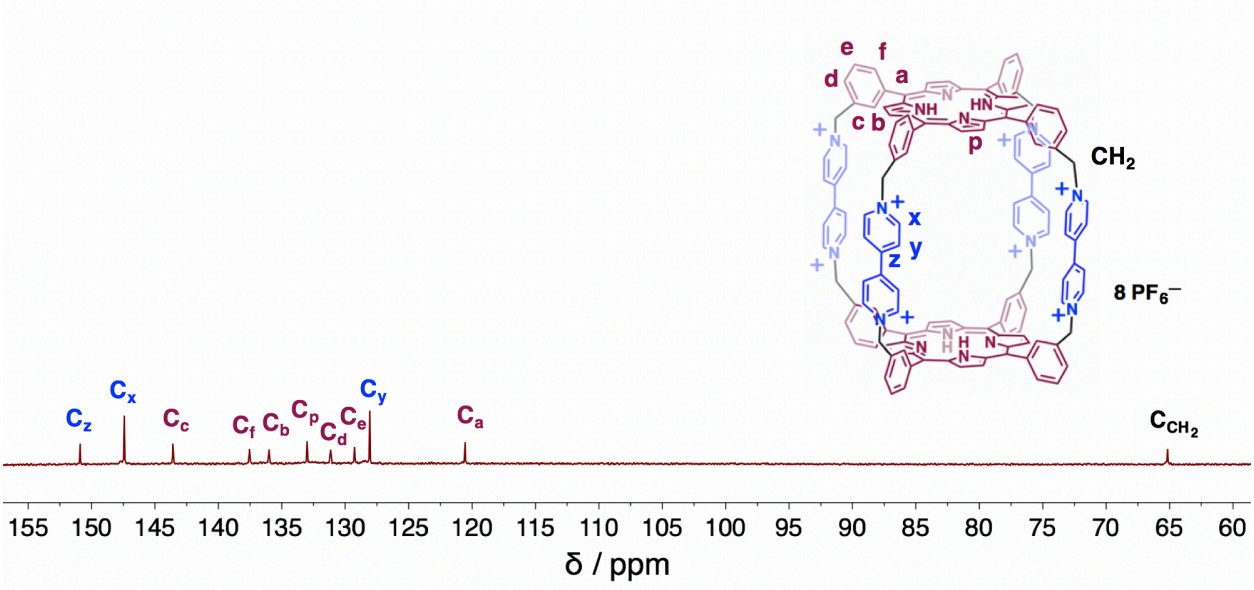

Figure S2. ^{13}C NMR Spectrum (125 MHz, DMF-d_7, 298 K) of **TPPCage**·8PF$_6$.

3) 2D NMR Spectra of TPPCage·8PF$_6$

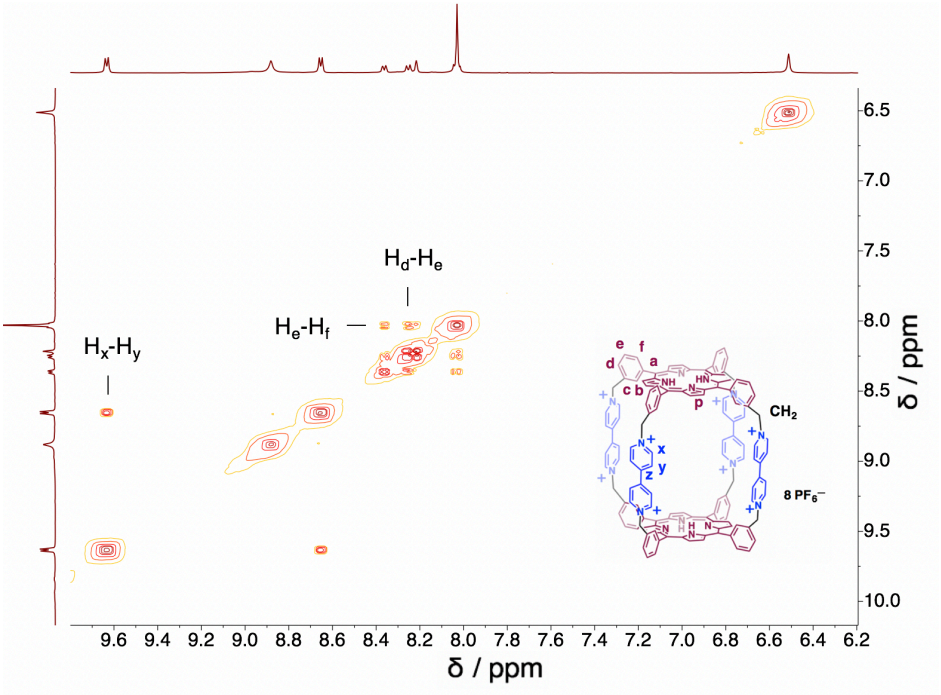

Figure S3. ^{1}H-^{1}H gCOSY NMR Spectrum (500 MHz, DMF-d_7, 298 K) of **TPPCage**·8PF$_6$.

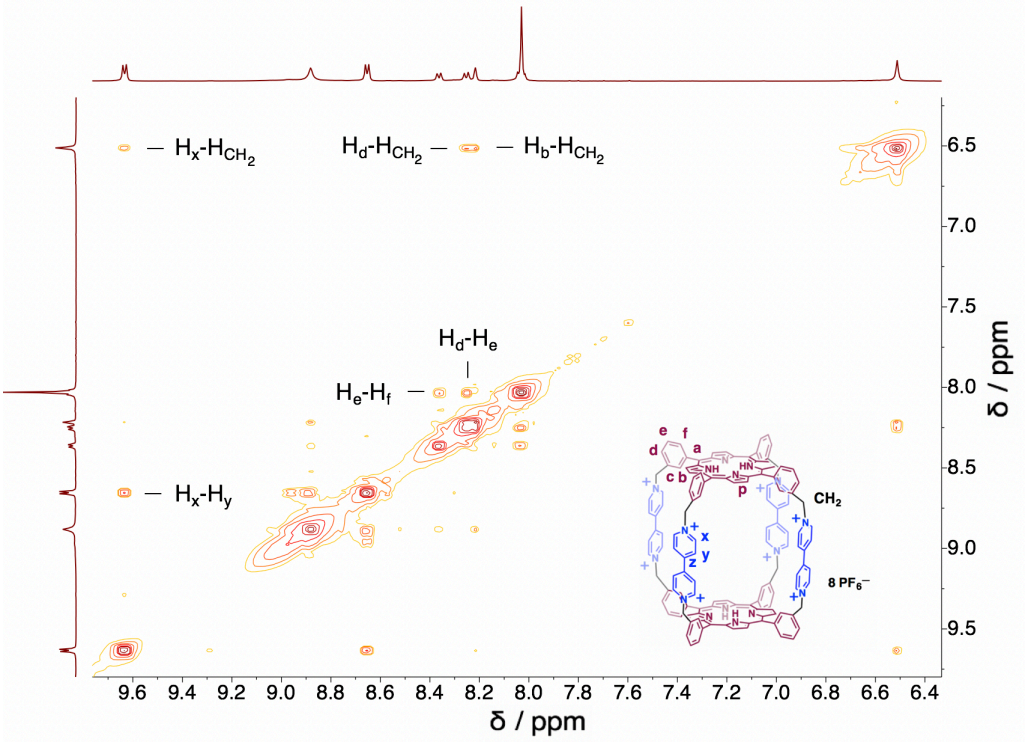

Figure S4. ^{1}H-^{1}H NOESY NMR Spectrum (500 MHz, DMF-d_7, 298 K) of **TPPCage**·8PF$_6$.

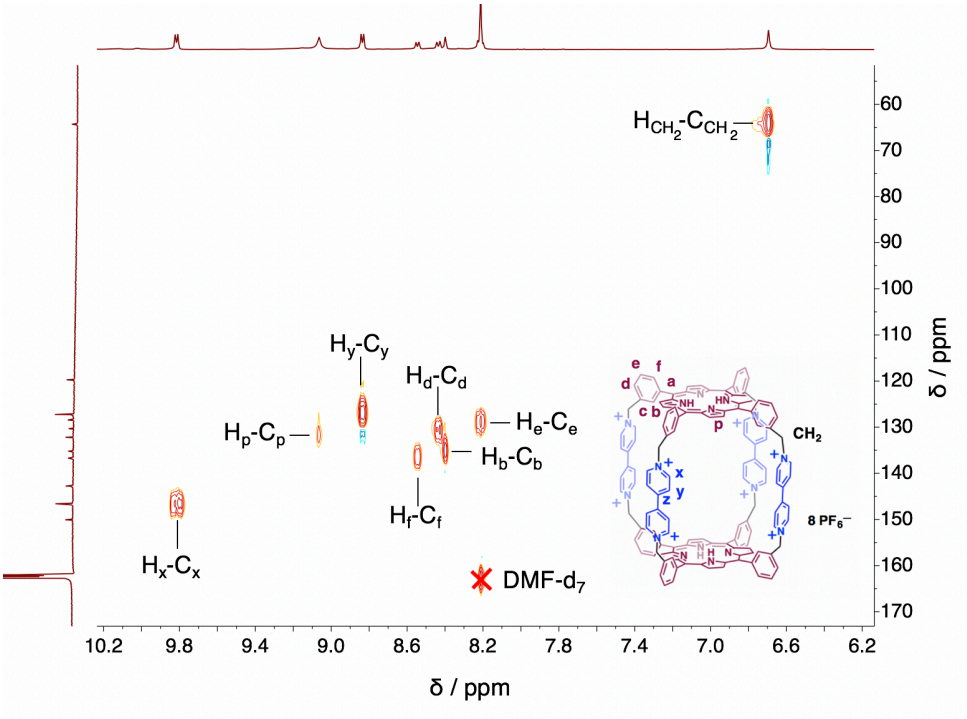

Figure S5. ^{1}H-^{13}C HSQC NMR Spectrum (DMF-d_7, 298 K) of **TPPCage**•8PF_6.

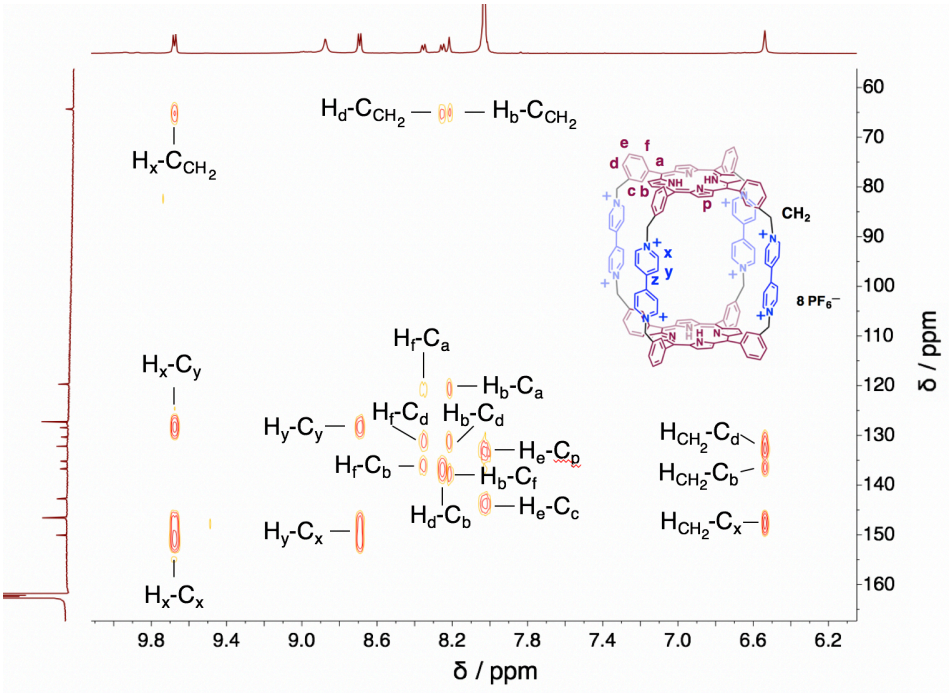

Figure S6. ^{1}H-^{13}C HMBC NMR Spectrum (DMF-d_7, 298 K) of **TPPCage**•8PF_6.

Section D. Host-Guest Studies of Complex of Fullerene⊂TPPCage·8PF$_6$

1) General Procedure for Fullerene Encapsulation

Fullerene was added to a solution of **TPPCage**•8PF$_6$ in DMF-d_7 (3.1 mg, 2 mM). After sonication at room temperature for 2 h, the undissolved solids were removed by centrifugation. The resulting solution was characterized by NMR spectroscopy and high-resolution mass spectrometry (HR-ESI).

2) Characterization for C_{60}⊂TPPCage·8PF$_6$ Complex

3.0 equiv of C_{60} was added to a solution of **TPPCage**•8PF$_6$ in DMF-d_7 (3.1 mg, 2 mM). The encapsulation was not complete even with excess of C_{60}, resulting a mixture of C_{60}⊂**TPPCage**•8PF$_6$ and **TPPCage**•8PF$_6$ in the solution.

C_{60}⊂TPPCage•8PF$_6$: ^{1}H NMR (500 MHz, $(CD_3)_2NCDO$, ppm) δ 9.75 (d, J = 6.6 Hz, 16H), 8.81 (s, 16 H), 8.72 (d, J = 6.6 Hz, 8H), 8.44 (d, J = 7.5 Hz, 8H), 8.26 – 8.22 (m, 8H), 8.07 (t, J = 7.7 Hz, 8H), 7.42 (s, 8H), 6.60 (s, 16H), -3.28 (s, 4H). ^{13}C NMR (125 MHz, $(CD_3)_2NCDO$, ppm): δ 151.0, 148.0, 144.1, 139.9, 136.6, 133.1, 132.4, 129.2, 128.3, 120.5, 65.2.

ESI-HRMS for C_{60}⊂**TPPCage**•8PF$_6$; Calcd for $C_{196}H_{100}F_{36}N_{16}P_6^{2+}$: m/z = 1774.3112 $[M - 2\,PF_6]^{2+}$; found: 1774.3122.

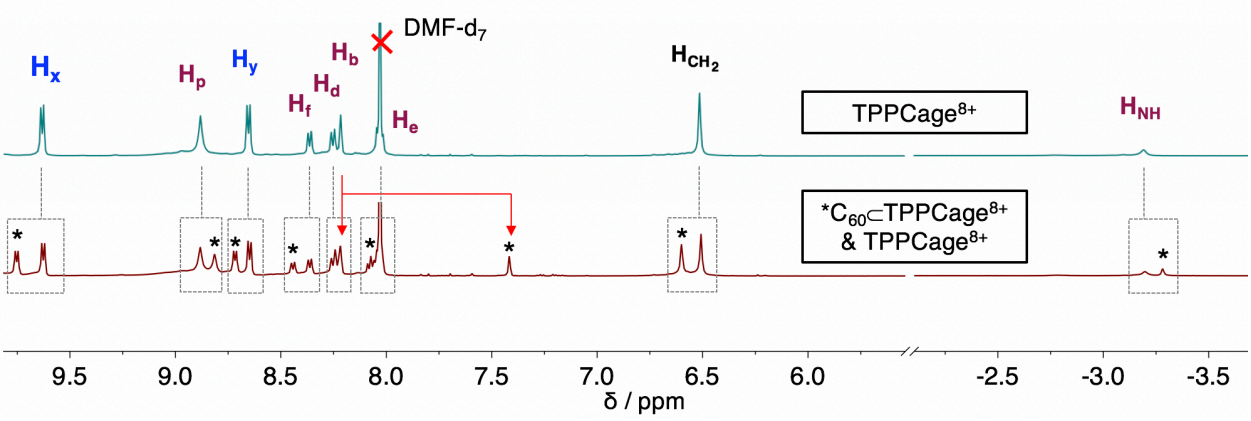

Figure S7. Stacked ^{1}H NMR Spectra (500 MHz, DMF-d_7, 298 K) Comparison of **TPPCage**•8PF$_6$ and C_{60}⊂**TPPCage**•8PF$_6$.

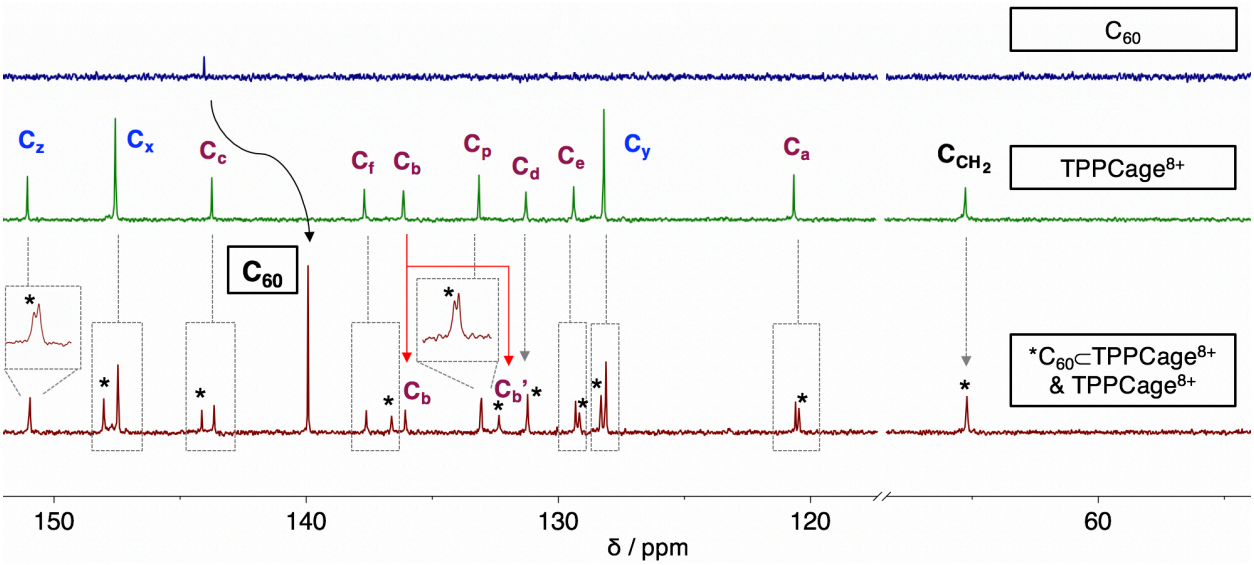

Figure S8. Stacked ^{13}C NMR Spectra (125 MHz, DMF-d_7, 298 K) Comparison of C_{60}, **TPPCage**•8PF_6 and C_{60}⊂**TPPCage**•8PF_6.

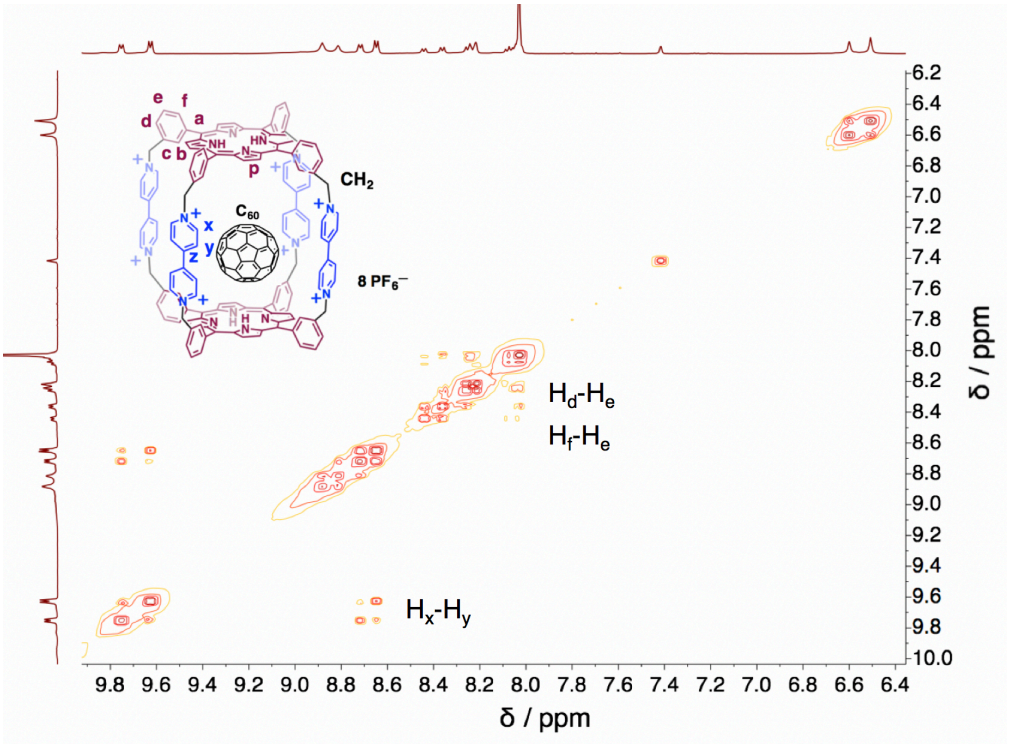

Figure S9. ^1H-^1H gCOSY NMR Spectrum (500 MHz, DMF-d_7, 298 K) of **TPPCage**•8PF_6 & C_{60}⊂**TPPCage**•8PF_6 mixture.

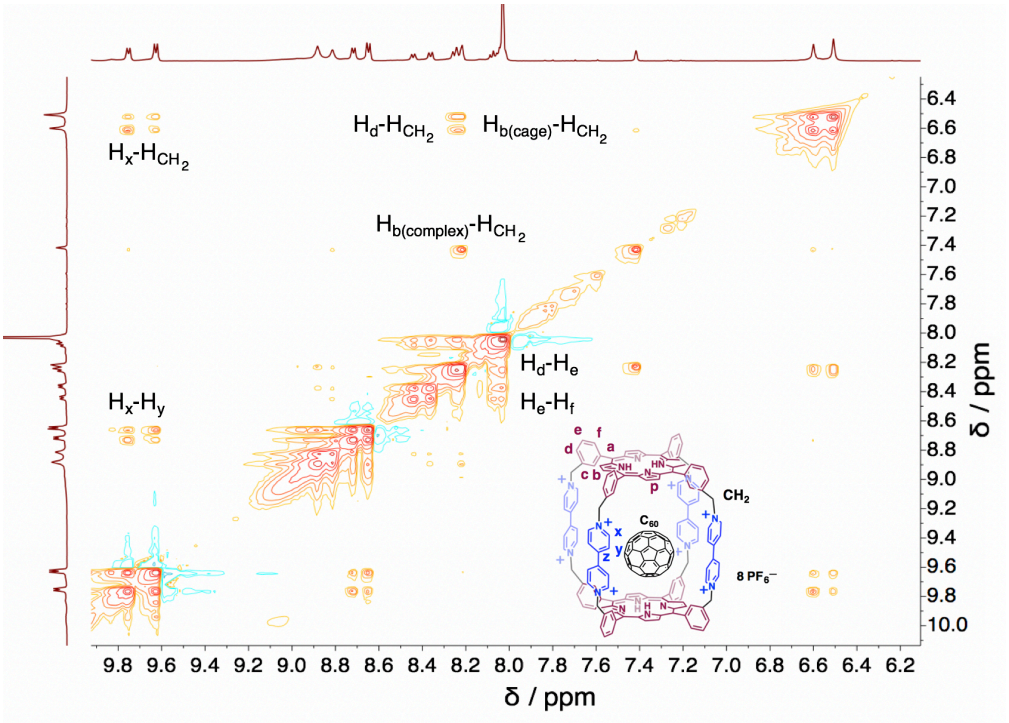

Figure S10. ^{1}H-^{1}H NOESY NMR Spectrum (500 MHz, DMF-d_7, 298 K) of **TPPCage**•8PF_6 & C_{60}⊂**TPPCage**•8PF_6 mixture.

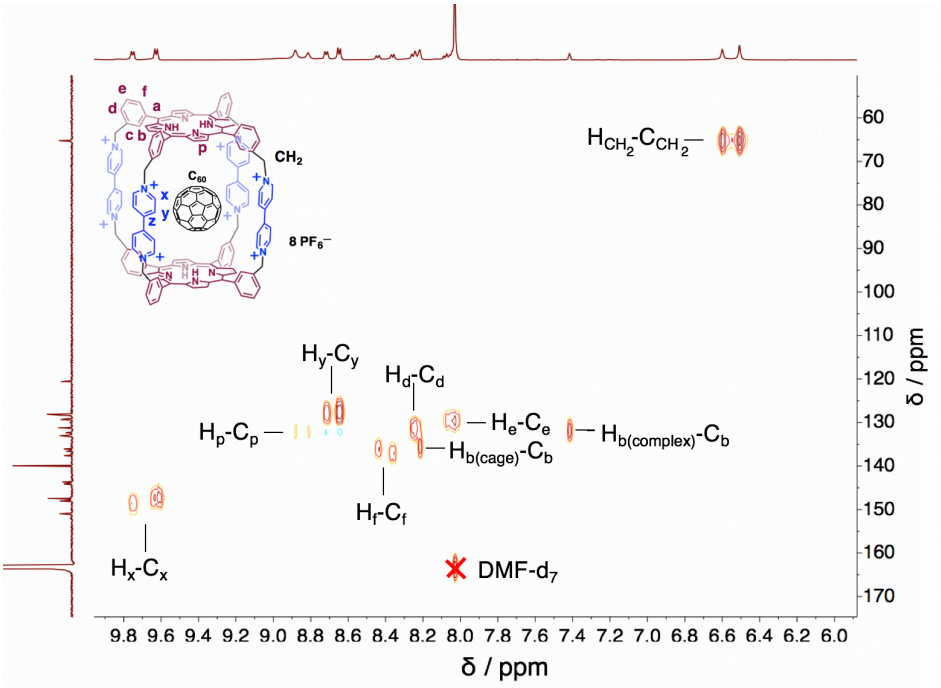

Figure S11. ^{1}H-^{13}C HSQC NMR Spectrum (DMF-d_7, 298 K) of **TPPCage**•8PF_6 & C_{60}⊂**TPPCage**•8PF_6 mixture.

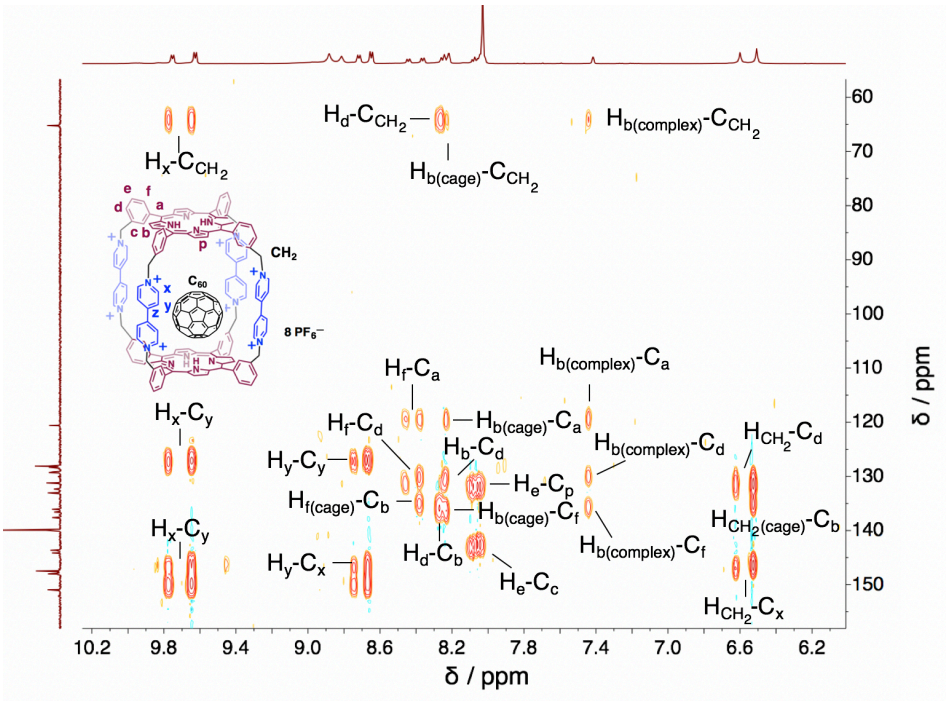

Figure S12. ^{1}H-^{13}C HMBC NMR Spectrum (DMF-d_7, 298 K) of **TPPCage**•8PF_6 & C_{60}⊂**TPPCage**•8PF_6 mixture.

3) Characterization for C_{70}⊂TPPCage•8PF_6 Complex

1.0 equiv of C_{70} was added to a solution of **TPPCage**•8PF_6 in DMF-d_7 (3.1 mg, 2 mM). The encapsulation was complete, resulting a solution of C_{70}⊂**TPPCage**•8PF_6 complex.

C_{70}⊂TPPCage•8PF_6: δ 9.76 (d, J = 6.7 Hz, 16H), 8.89 (d, J = 6.7 Hz, 16H), 8.79 (s, 16 H), 8.32 (d, J = 7.5 Hz, 8H), 8.25 (d, J = 8.0 Hz, 8H), 8.05 – 8.02 (m, 8H), 7.65 (s, 8H), 6.61 (s, 16H), -3.73 (s, 4H). ^{13}C NMR (125 MHz, $(CD_3)_2$NCOD, ppm): δ 150.7, 149.2, 148.0, 145.4, 1445.0, 144.0, 141.8, 137.6, 133.0, 132.8, 131.7, 129.2, 128.4, 127.0, 120.6, 65.4. ESI-HRMS for C_{70}⊂**TPPCage**•8PF_6; Calcd for $C_{206}H_{100}F_{36}N_{16}P_6^{2+}$: m/z = 1834.3112 $[M - 2\ PF_6]^{2+}$; found: 1834.3094.

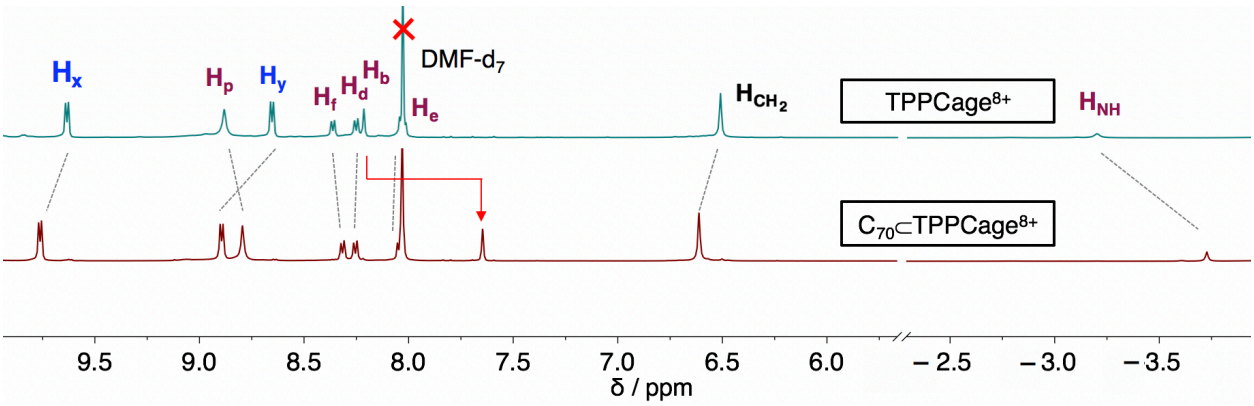

Figure S13. Stacked ^{1}H NMR Spectra (500 MHz, DMF-d_7, 298 K) Comparison of **TPPCage**·8PF_6 and C_{70}⊂**TPPCage**·8PF_6.

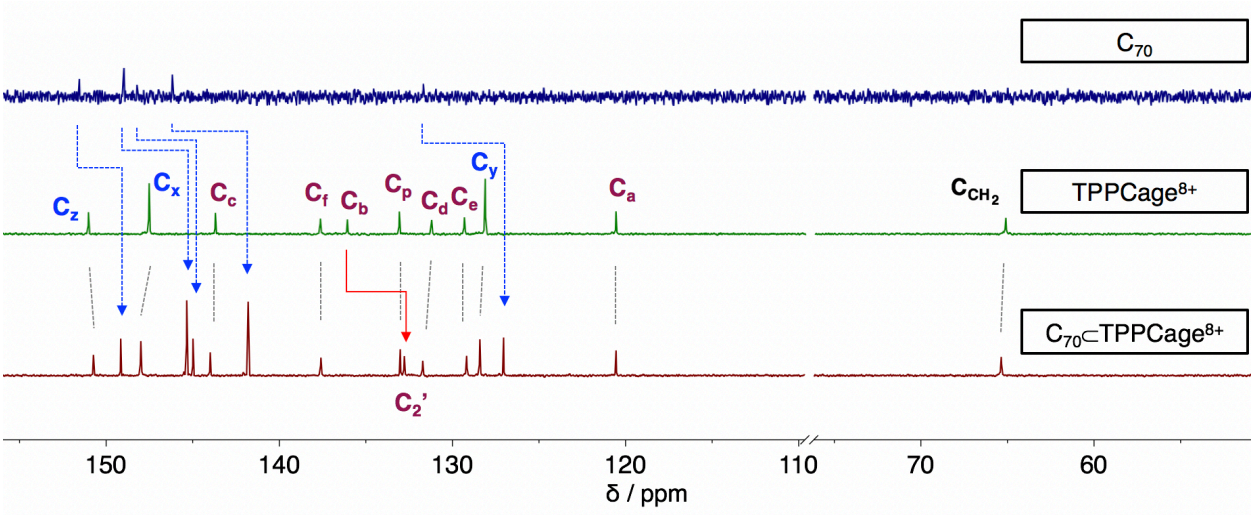

Figure S14. Stacked ^{13}C NMR Spectra (125 MHz, DMF-d_7, 298 K) Comparison of C_{70}, **TPPCage**·8PF_6 and C_{70}⊂**TPPCage**·8PF_6.

Compound	δ / ppm				
Free C_{70}	150.6	148.0	147.3	145.2	130.8
C_{70} in complex	149.2	145.4	145.0	144.0	127.0

Table S1. Chemical shift comparison between free C_{70} and C_{70} in complex in ^{13}C NMR Spectra at 298 K (125 MHz, DMF-d_7, ~1 mM for **TPPCage**·8PF_6)

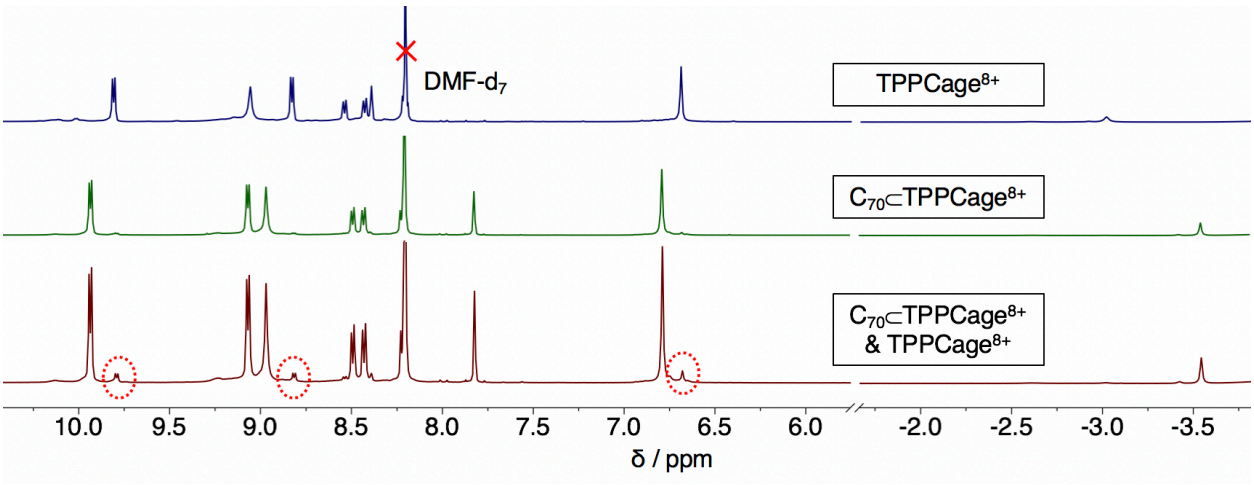

Figure S15. Stacked ^{1}H NMR Spectra (500 MHz, DMF-d_7, 298 K) Comparison of **TPPCage**•8PF$_6$, C$_{70}$⊂**TPPCage**•8PF$_6$ (complete encapsulation) and a mixture of **TPPCage**•8PF$_6$ and C$_{70}$⊂**TPPCage**•8PF$_6$ (90% encapsulation), indicating a slow exchange in DMF at room temperature (~1 mM for **TPPCage**•8PF$_6$).

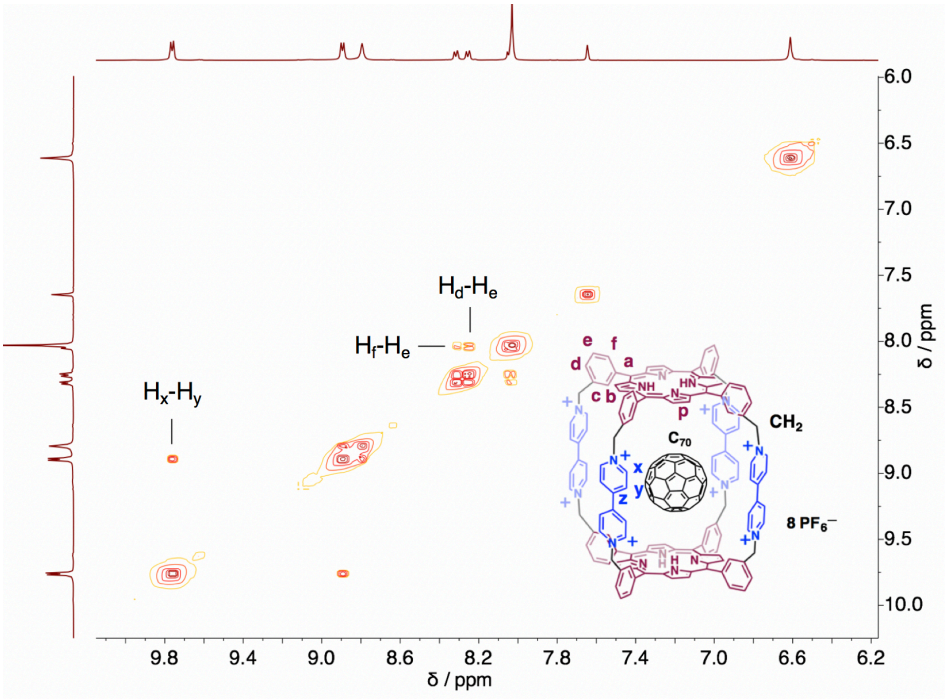

Figure S16. ^{1}H-^{1}H gCOSY NMR Spectrum (500 MHz, DMF-d_7, 298 K) of C$_{70}$⊂**TPPCage**•8PF$_6$.

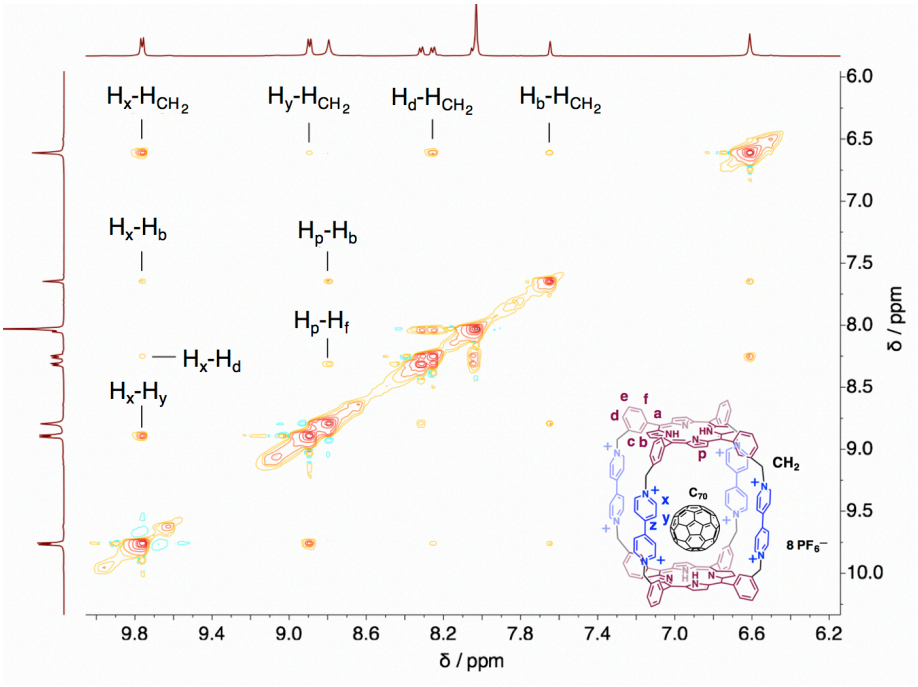

Figure S17. ^{1}H-^{1}H NOESY NMR Spectrum (500 MHz, DMF-d_7, 298 K) of C_{70}⊂**TPPCage**•8PF_6.

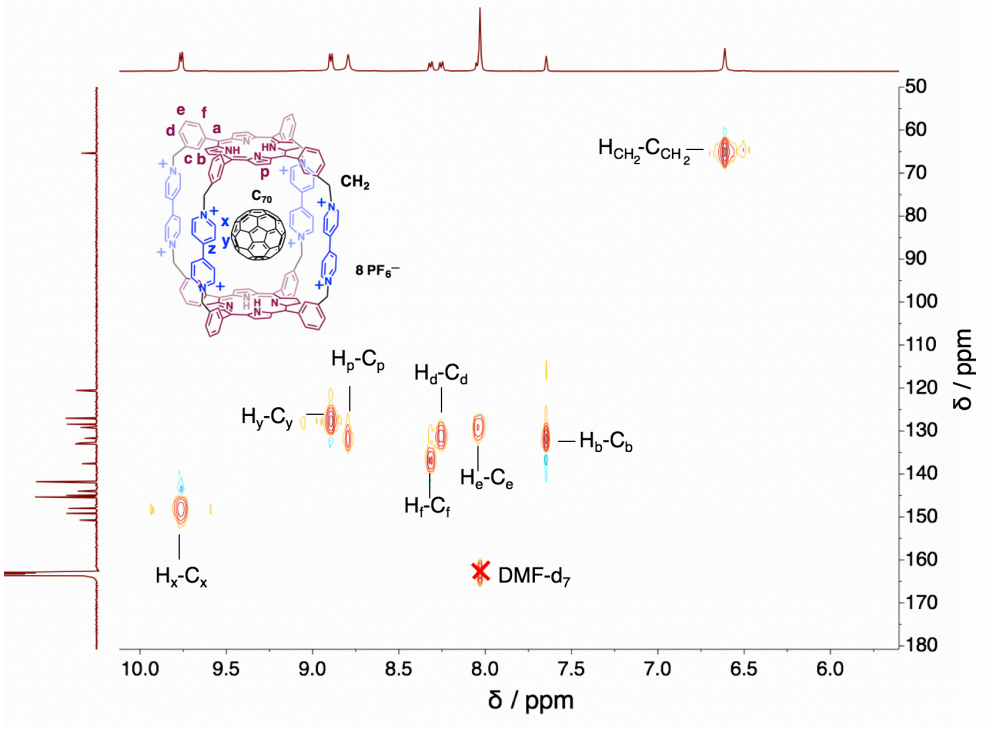

Figure S18. ^{1}H-^{13}C HSQC NMR Spectrum (DMF-d_7, 298 K) of C_{70}⊂**TPPCage**•8PF_6.

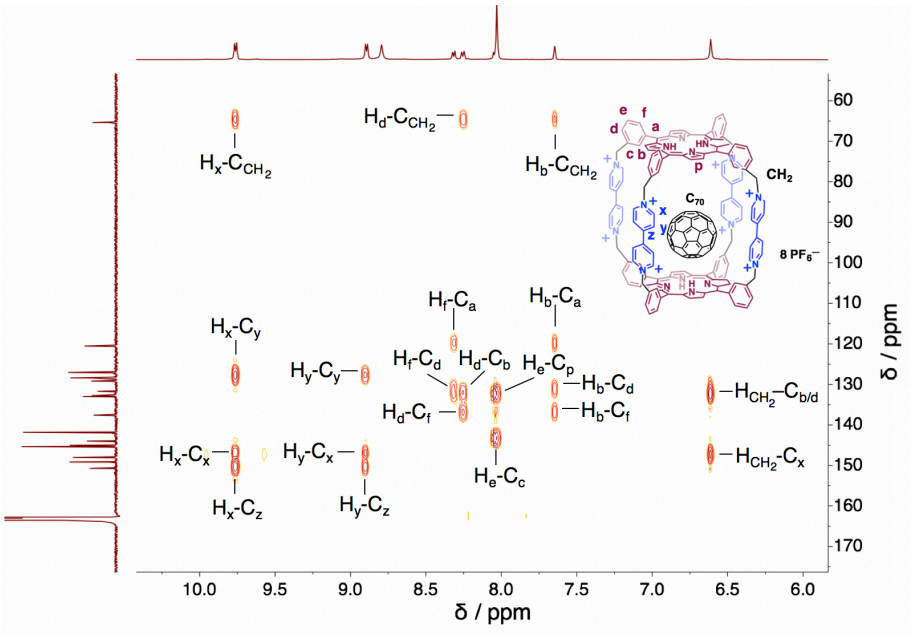

Figure S19. ^{1}H-^{13}C HMBC NMR Spectrum (DMF-d_7, 298 K) of C_{70}⊂**TPPCage**•8PF_6.

4) Selective Extraction of C_{70}

A mixture of fullerene C_{60} (10 μmol) and C_{70} (1 μmol) was added to a solution of **TPPCage**•8PF_6 in DMF-d_7 (1 μmol, 3.1 mg, 2 mM). The selective encapsulation of C_{70} was achieved, resulting in a solution of C_{70}⊂**TPPCage**•8PF_6 complex.

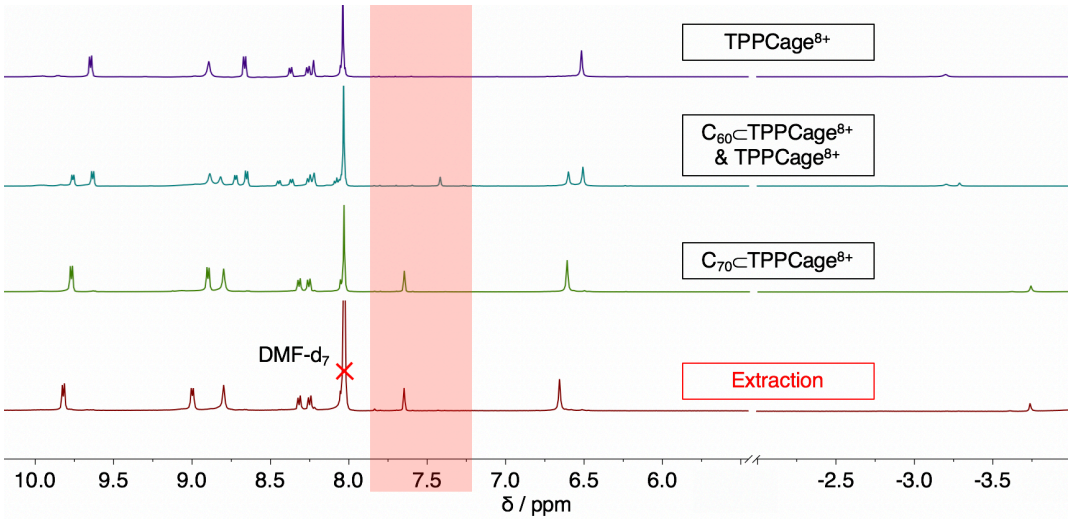

Figure S20. Stacked ^{1}H NMR Spectra (500 MHz, DMF-d_7, 298 K) Comparison of **TPPCage**•8PF_6, **TPPCage**•8PF_6 & C_{60}⊂**TPPCage**•8PF_6, C_{70}⊂**TPPCage**•8PF_6, and C_{70} Extraction Solution.

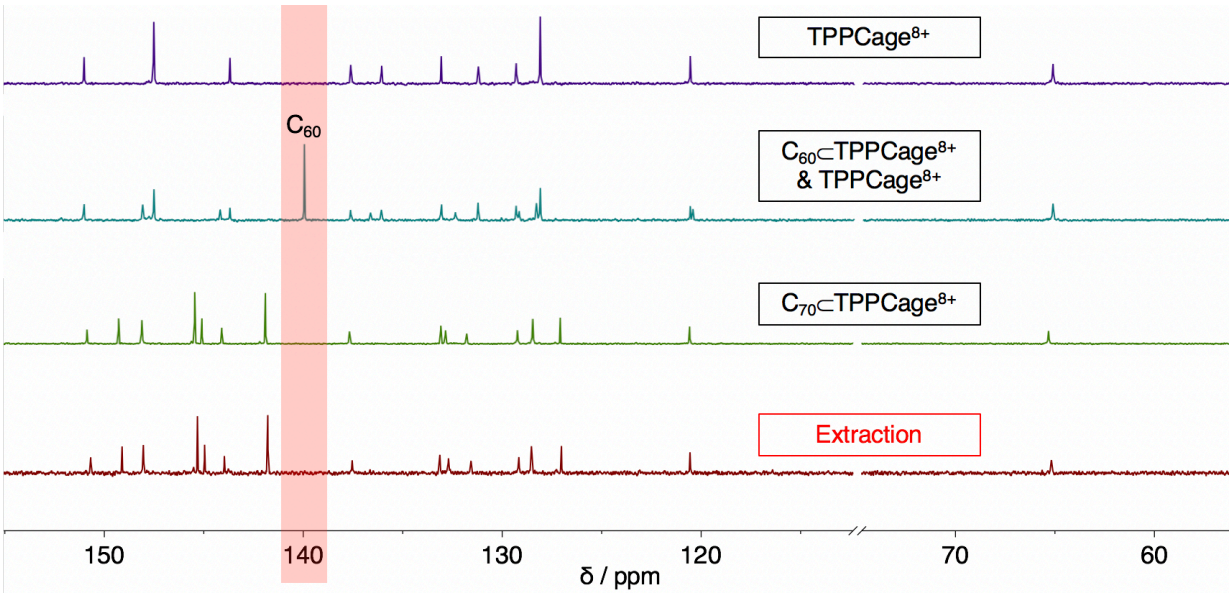

Figure S21. Stacked ^{13}C NMR Spectra (125 MHz, DMF-d_7, 298 K) Comparison of **TPPCage**•8PF_6, **TPPCage**•8PF_6 & C_{60}⊂**TPPCage**•8PF_6, C_{70}⊂**TPPCage**•8PF_6, and C_{70} Extraction Solution.

Section E. DOSY NMR Experiment

A DOSY NMR experiment was carried out with Bruker Avance III 600 MHz spectrometer. The effective hydrodynamic radius R was calculated from the Stokes-Einstein equation, $D=(k_BT)/(6\pi\eta r)$, where D is the diffusion coefficient, k_B is the Boltzmann constant, T is the absolute temperature, and η is the viscosity of the DMF-d_7 (0.86 mPa·s).

1) TPPCage•8PF_6

The measured diffusion coefficient is 2.12 × 10^{-6} cm^2s^{-1}, and the hydrodynamic radius of **TPPCage**•8PF_6 is calculated to be 12.0 Å.

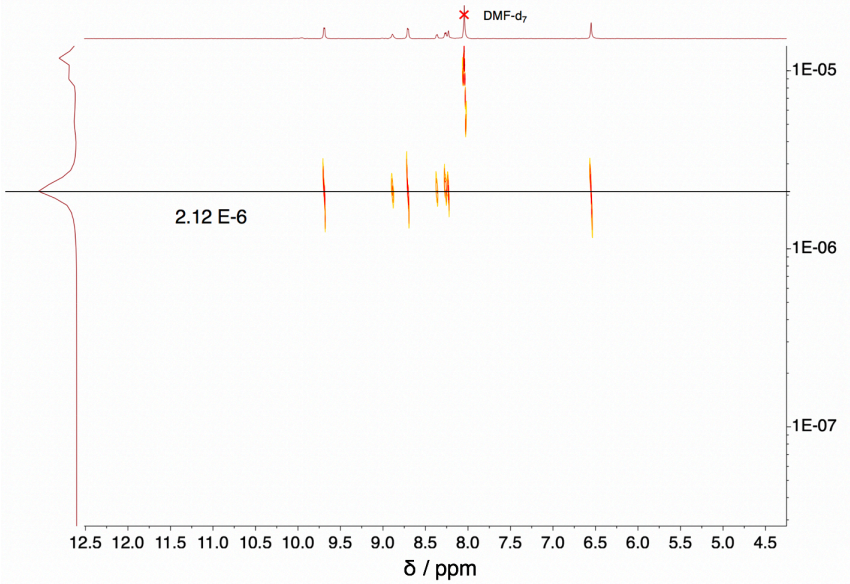

Figure S22. gDOSY NMR Spectrum (600 MHz, DMF-d_7, 298 K) of **TPPCage**•$8PF_6$.

2) C_{60} ⊂ TPPCage•8PF_6

The measured diffusion coefficient is 2.09 E-6 cm^2s^{-1}, and the hydrodynamic radius of C_{60}⊂**TPPCage**•$8PF_6$ is calculated to be 12.1 Å.

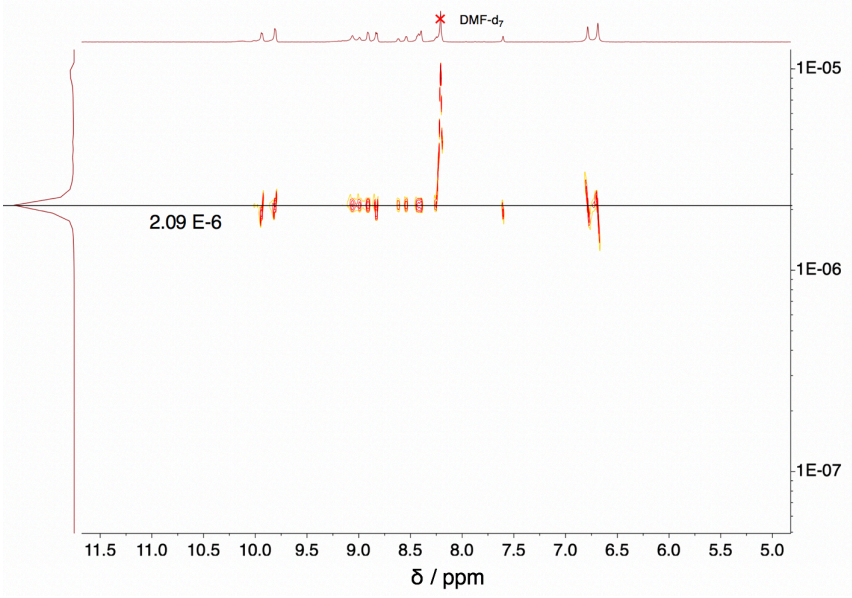

Figure S23. gDOSY NMR Spectrum (600 MHz, DMF-d_7, 298 K) of C_{60}⊂**TPPCage**•$8PF_6$ and **TPPCage**•$8PF_6$ mixture.

3) C_{70} ⊂ TPPCage·8PF$_6$

The measured diffusion coefficient is 2.10 E-6 cm^2s^{-1}, and the hydrodynamic radius of C_{70}⊂**TPPCage**•8PF_6 is calculated to be 12.1 Å.

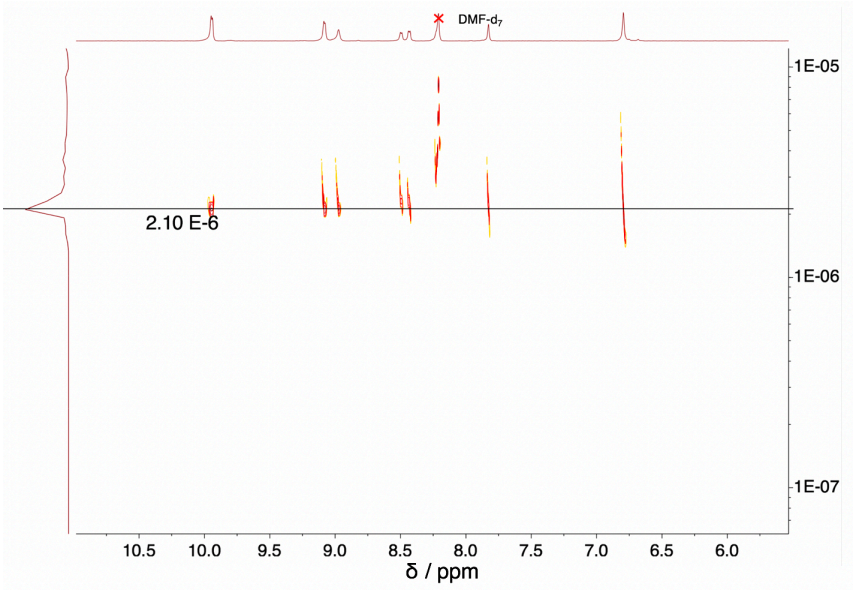

Figure S24. gDOSY NMR Spectrum (600 MHz, DMF-d_7, 298 K) of C_{70}⊂**TPPCage**•8PF_6.

Section F. Binding Constant Determination

1) NMR Spectra Integration of TPPCage·8PF$_6$ and C_{60}⊂TPPCage·8PF$_6$

The binding constant (K_a) for the formation of C_{60}⊂**TPPCage**•8PF_6 complex in DMF was determined by NMR spectroscopy from 3 parallel experiments. An excess of C_{60} (3.0 equiv) was added to a solution of **TPPCage**•8PF_6 in DMF-d_7 (0.5 mM, 1 mM, 2 mM). After sonication for 2 h, the mixture was allowed to stand at room temperature for another 5 h to make sure it reached equilibrium. The undissolved solids were removed by centrifugation, resulting a solution of C_{60}⊂**TPPCage**•8PF_6 and **TPPCage**•8PF_6 (the encapsulation was not complete even with large excess of C_{60}). The binding constant was calculated based on equation

$$K_a = [C_{60}\subset\textbf{TPPCage}\bullet 8PF_6] / ([\textbf{TPPCage}\bullet 8PF_6] \times [C_{60}])$$

where $[C_{60}\subset\textbf{TPPCage}\bullet 8PF_6] / [\textbf{TPPCage}\bullet 8PF_6]$ can be obtained from NMR spectra integration (average of signal H_a, H_b, H_6, H_{CH2}), and the concentration of saturated C_{60} in DMF can be measured from UV-Vis spectra.[S1]

Table S2. Binding Constant Determination for $C_{60}\subset\textbf{TPPCage}\bullet 8PF_6$.

$[C_{60}]$ [a]	1.58×10^{-4} M		
$[C_{60}\subset\textbf{TPPCage}\bullet 8PF_6] / ([\textbf{TPPCage}\bullet 8PF_6]$ [b]	0.64	0.77	0.72
Average Ratio [c]	0.71		
K_a	$(4.5 \pm 0.4) \times 10^3$ M^{-1}		

[a] C_{60} is saturated in DMF in all 3 experiments, and the concentration was measured from its UV-Vis spectra. [b] The ratio between $C_{60}\subset\textbf{TPPCage}\bullet 8PF_6$ complex and empty $\textbf{TPPCage}\bullet 8PF_6$ was calculated according to NMR spectra integration. [c] Average ratio calculated from 3 parallel experiments.

2) UV-Vis Titration of TPPCage·8PF$_6$ with C$_{70}$

The binding constant (K_a) for the formation of $C_{70}\subset\textbf{TPPCage}\bullet 8PF_6$ complex in DMF was determined by UV titration on a Shimadzu UV-3600 spectrophotometer using 0.2 cm UV cuvette. The concentrated solution of C_{70} (1 mM in PhMe) was added incrementally to the solution $\textbf{TPPCage}\bullet 8PF_6$ (10 μM in DMF). The UV-Vis spectra were recorded one after the other. The stacked spectra (Figure S25) show that, upon the addition of C_{70}, the absorption band on centered on 419 nm was reduced and slightly shifted to 422 nm. From the UV-Vis titration experiment, a plot (Figure S25, black dot) of absorption intensity at 419-422 nm against the equiv of C_{70} was

obtained and a non-linear least squares data treatment[S2] (Figure S25, red line) gave an association constant of $(2.4 \pm 0.2) \times 10^5\ M^{-1}$.

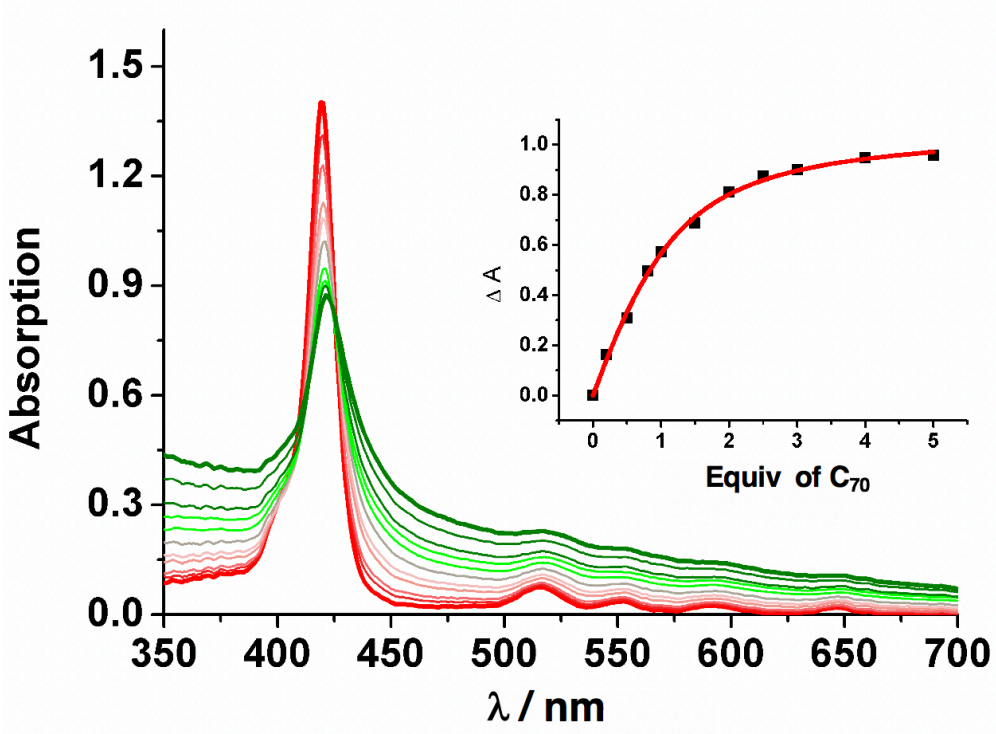

Figure S25. UV-Vis Spectrophotometric monitoring of the titration of a solution of **TPPCage**•$8PF_6$ (10 μM in DMF) with C_{70} (1 mM in PhMe) in a 0.2 cm path cuvette. Inset: plot of ΔA422 nm vs equivalents of C_{70} added. The association constants modeled with a 1:1 equilibrium are $K_{C70\subset TPPCage} = (2.4 \pm 0.2) \times 10^5\ M^{-1}$.

Section H. Crystallographic Characterization

All crystallographic data are available free of charge from the Cambridge Crystallographic Data Centre via www.ccdc.cam.ac.uk/data_request/cif.

1) TPPCage•8PF₆

a) Methods. **TPPCage**•$8PF_6$ (2 mg) was dissolved in MeCN (1.0 mL) and the mixture was passed through a 0.45-µm filter into VWR culture tubes. The tubes were placed in one 20-mL vial

containing $^{i}Pr_2O$ (~3 mL) and the vial was capped. Slow vapor diffusion of $^{i}Pr_2O$ into the solution of **TPPCage•**$8PF_6$ in MeCN (0.6 mM) over the course of 4 d yielded brown needle-like single crystals of **TPPCage•**$8PF_6$. A suitable crystal was selected and the crystal was mounted on a MITIGEN holder in Paratone oil on a Kappa Apex 2 diffractometer. The crystal was kept at 99.99 K during data collection. Using Olex2[S3], the structure was solved with the ShelXT[S4] structure solution program using Intrinsic Phasing and refined with the XL[S5] refinement package using Least Squares minimization. The solid-state structure of **TPPCage•**$8PF_6$ is shown in Figure S26a.

b) Crystal data. Monoclinic, space group $P2_1/c$ (no. 14), a = 15.8431(11), b = 16.2840(10), c = 34.474(2) Å, β = 91.307(4)°, V = 8891.6(10) Å^3, Z = 2, T = 99.99 K, μ(CuKα) = 1.654 mm^{-1}, D_{calc} = 1.318 g/mm^3, 45595 reflections measured (7.468 ≤ 2Θ ≤ 127.59), 14527 unique (R_{int} = 0.0495, R_{sigma} = 0.0512) which were used in all calculations. The final R_1 was 0.0925 ($I > 2\sigma(I)$) and wR_2 was 0.2995 (all data).

c) Refinement details. Distance restraints were imposed on the disordered PF_6^- anions and the hydrogens on the nitrogens in the porphyrin. The enhanced rigid-bond restraint (SHELX keyword RIGU) was applied globally.

d) Solvent treatment details. The solvent masking procedure as implemented in Olex2 was used to remove the electronic contribution of solvent molecules from the refinement. As the exact solvent content is not known, only the atoms used in the refinement model are reported in the formula here. Total solvent accessible volume / cell = 1365.9 Å^3 [15.4%] Total electron count / cell = 288.2.

2) C_{60}⊂TPPCage•$8PF_6$

a) Methods. A solution of **TPPCage•**$8PF_6$ (1 mg) in DMF (0.5 mL) and a solution of C_{60} (~0.3 mg) in PhMe (0.5 mL) were mixed, the mixture was passed through a 0.45-μm filter into VWR culture tubes. The tubes were placed in one 20-mL vial containing $^{i}Pr_2O$ (~3 mL) and the vial was

capped. Slow vapor diffusion of $^{i}Pr_2O$ into the solution of C_{60} and **TPPCage•**$8PF_6$ in 1:1 DMF/PhMe over the period of 7 d yielded dark brown single crystals of C_{60}⊂**TPPCage•**$8PF_6$. A suitable crystal was selected and the crystal was mounted on a MITIGEN holder in Paratone oil on a Kappa Apex 2 diffractometer. The crystal was kept at 100.0 K during data collection. Using Olex2[S3], the structure was solved with the XM[S5] structure solution program using Dual Space and refined with the XL[S5] refinement package using Least Squares minimisation. The solid-state superstructure of C_{60} ⊂ **TPPCage•**$8PF_6$ is shown in Figure S26b.

b) Crystal data. Monoclinic, space group *C*2/*c* (no. 15), $a = 26.125(4)$, $b = 22.632(4)$, $c = 35.143(5)$ Å, $\beta = 109.353(10)°$, $V = 19604(5)$ Å^3, $Z = 4$, $T = 100.0$ K, μ(CuKα) = 1.569 mm^{-1}, $D_{calc} = 1.350$ g/mm^3, 34816 reflections measured ($5.33 \leq 2\Theta \leq 88.984$), 7704 unique ($R_{int} = 0.1612$, $R_{sigma} = 0.1196$) which were used in all calculations. The final R_1 was 0.0915 ($I > 2\sigma(I)$) and wR_2 was 0.3064 (all data).

c) *Refinement details*. Distance restraints were imposed on the disordered PF_6^- molecule as well as the enhanced rigid-bond restraint (SHELX keyword RIGU).

d) *Solvent treatment details.* The solvent masking procedure as implemented in Olex2 was used to remove the electronic contribution of solvent molecules from the refinement. As the exact solvent content is not known, only the atoms used in the refinement model are reported in the formula here. Total solvent accessible volume / cell = 3915.6 Å^3 [20.0%] Total electron count / cell = 1220.0.

3) C_{70}⊂TPPCage•$8PF_6$

a) Methods. A solution of **TPPCage•**$8PF_6$ (1 mg) in DMF (0.5 mL) and a solution of C_{70} (~0.3 mg) in PhMe (0.5 mL) were mixed, the mixture was passed through a 0.45-μm filter into VWR

culture tubes. The tubes were placed in one 20-mL vial containing $^{i}Pr_2O$ (~3 mL) and the vial was capped. Slow vapor diffusion of $^{i}Pr_2O$ into the solution of C_{70} and **TPPCage•**$8PF_6$ in 1:1 DMF/PhMe over the period of 14 d yielded dark brown single crystals of C_{70}⊂**TPPCage•**$8PF_6$. A suitable crystal was selected and the crystal was mounted on a MITIGEN holder in Paratone oil on a Bruker Kappa APEX CCD area detector diffractometer. The crystal was kept at 100.0 K during data collection. Using Olex2 [S3], the structure was solved with the XM[S5] structure solution program using Dual Space and refined with the XL[S5] refinement package using Least Squares minimization. The solid-state superstructure of C_{70} ⊂ **TPPCage•**$8PF_6$ is shown in Figure S26c.

b) Crystal data. Trigonal, space group $P3_121$ (no. 152), a = 23.6016(8), c = 61.756(2) Å, V = 29791(2) Å^3, Z = 6, T = 100.0 K, μ(CuKα) = 1.567 mm^{-1}, D_{calc} = 1.373 g/mm^3, 129409 reflections measured ($4.322 \leq 2\Theta \leq 127.444$), 32729 unique ($R_{int}$ = 0.0448, R_{sigma} = 0.0430) which were used in all calculations. The final R_1 was 0.1479 ($I > 2\sigma(I)$) and wR_2 was 0.4184 (all data).

c) Refinement details. The disordered C_{70} was placed in an idealized positions and the second residue was refined with similar bond lengths. Distance restraints were imposed on the PF_6^- anions as well as the disordered ring. The enhanced rigid-bond restraint (SHELX keyword RIGU) was applied the same anions and disordered ring as well as the solvent molecules.

d) Solvent treatment details. The solvent masking procedure as implemented in Olex2 was used to remove the electronic contribution of solvent molecules from the refinement. As the exact solvent content is not known, only the atoms used in the refinement model are reported in the formula here. Total solvent accessible volume / cell = 6059.8 Å^3 [20.3%] Total electron count / cell = 1727.1.

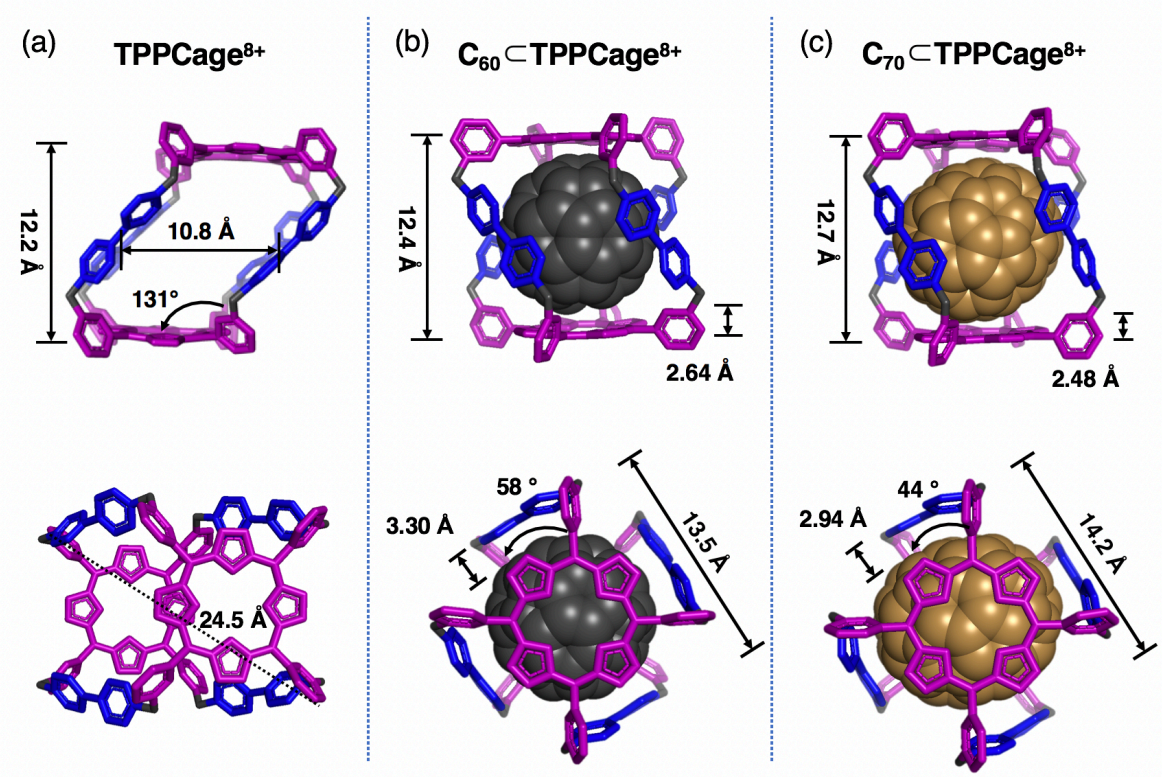

Figure S26. Solid-state (super)structure of (a) **TPPCage**$^{8+}$, (b) C_{60}⊂**TPPCage**$^{8+}$, and (c) C_{70}⊂**TPPCage**$^{8+}$ obtained from single crystal X-ray diffraction. PF_6^- anions and solvent molecules are omitted for the sake of clarity.

Table S3. Summary of measured distances and angles from the solid-state (super)structures of **TPPCage**$^{8+}$, C_{60}⊂**TPPCage**$^{8+}$, and C_{70}⊂**TPPCage**$^{8+}$.

	TPPCage^{8+}	C_{60}⊂**TPPCage**$^{8+}$	C_{70}⊂**TPPCage**$^{8+}$
Torsion angle φ / °	0	58	44
Height of cage / Å	12.2	12.4	12.7
Fullerene to porphyrin / Å	N/A	2.64	2.48
Fullerene to viologen / Å	N/A	3.3	2.94

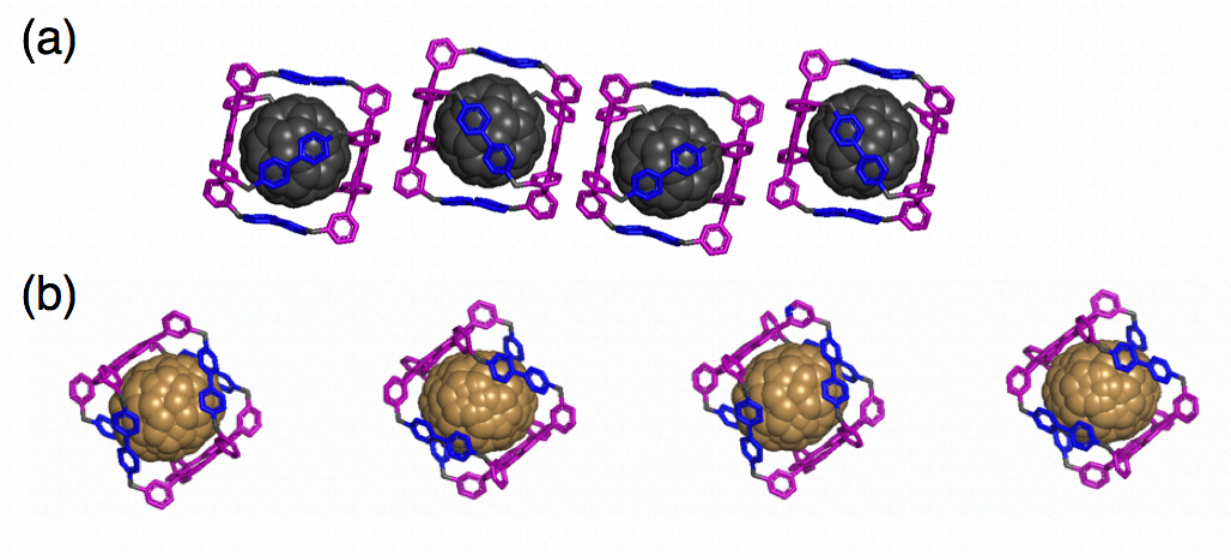

Figure S27. Solid-state superstructure of fullerene⊂**TPPCage**$^{8+}$ revealing a racemic packing by the chiral host-guest complex.

Section I. DFT Calculations

Computational Details. All DFT calculations were performed using the ORCA package.[S6] The valence double-zeta basis sets def2-SVP were used for geometry optimization, and the valence triple-zeta basis sets def2-TZVP(-f) were used for computing the final energies from single-point calculations upon geometries optimized with B3LYP-D3/def-SVP. The resolution of identity RIJCOSX approximation was used to accelerate both the B3LYP-D3 and M06-2X calculations. The solvation effect was taken into account using the conductor-like continuum polarization model[S7] (C-PCM) with DMF as the solvent. The encapsulation energy is defined as the energy difference between the host cage molecule plus the guest molecule and the encapsulated host-guest complex.

Table S4. Encapsulation energies (in kcal/mol) for the C_{60} and C_{70} cases.

Guest	B3LYP	dispersion (D3)	B3LYP-D3	M06-2X
C_{60}	–24.4	70.2	45.8	21.2
C_{70}	–39.5	100.5	60.9	25.4

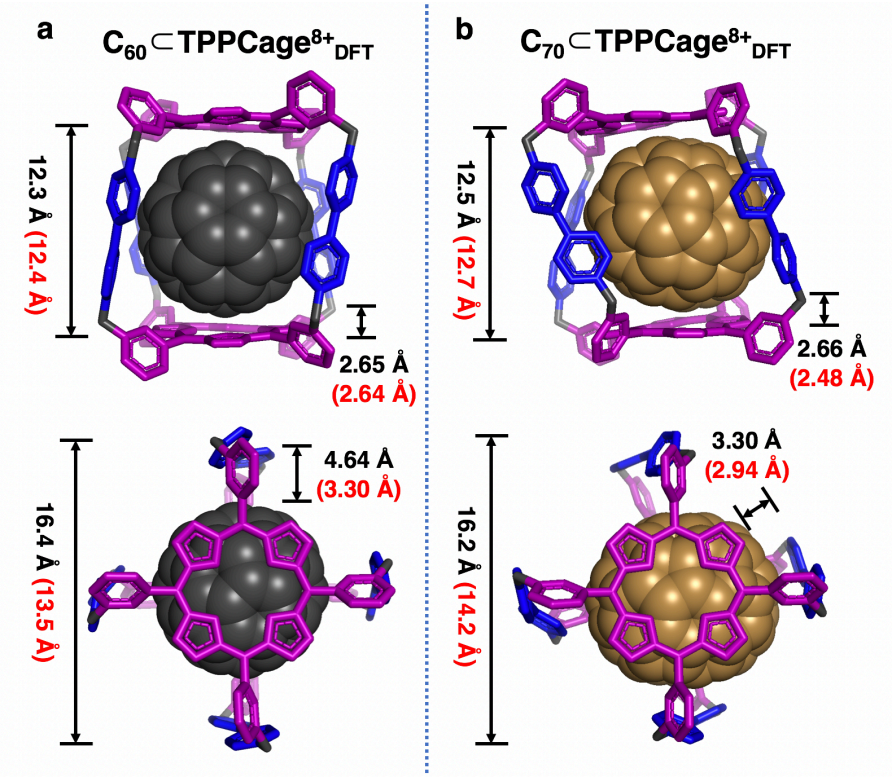

Figure S28. Optimized computational model (super)structures of (a) C_{60}⊂**TPPCage**$^{8+}{}_{DFT}$, and (b) C_{70}⊂**TPPCage**$^{8+}{}_{DFT}$ determined by DFT calculations employing the B3LYP functional with empirical D3 dispersion correction (B3LYP-D3), and the M06-2X functional that includes dispersion intrinsically. Distances from the DFT optimized structures are provided in black, and the corresponding measurements from the solid-state structures are presented in red in parentheses.

Section J. References

(S1) Hare, J. P.; Kroto, H. W.; Taylor, R. *Chem. Phys. Lett.* **1991**, *177*, 394-398. (b) Sivaraman, N.; Dhamodaran, R.; Kaliappan, I.; Srinivasan, T. G.; Vasudeva Rao, P. R. P.; Mathews, C. K. C., *Fullerene Sci. Technol.* **1994**, *2*, 233–246.

(S2) Thordarson, P. *Chem. Soc. Rev.* **2011**, *40*, 1305–1323.

(S3) Dolomanov, O. V.; Bourhis, L. J.; Gildea, R. J.; Howard, J. A. K.; Puschmann, H.; *J. Appl. Cryst.* **2009**, *42*, 339–341.

(S4) Sheldrick, G. M. *Acta Cryst.* **2015**, *A71*, 3–8.

(S5) Sheldrick, G. M. *Acta Cryst.* **2008**, *A64*, 112–122.

(S6) Neese, F., The ORCA Program System. *Wiley Interdiscip. Rev.: Comput. Mol. Sci.* **2012,** *2* (1), 73–78.

(S7) Barone, V.; Cossi, M., Quantum Calculation of Molecular Energies and Energy Gradients in Solution by a Conductor Solvent Model. *J. Phys. Chem. A* **1998,** *102*, 1995–2001.